AIMS Materials Science, 7(3): 244–268.
DOI: 10.3934/matersci.2020.3.244
Received: 08 February 2020
Accepted: 14 May 2020
Published: 27 May 2020

http://www.aimspress.com/journal/Materials

Review

A review on structural, electrical and magnetic properties of Y-type hexaferrites synthesized by different techniques for antenna applications and microwave absorbing characteristic materials

Monika Chandel[1], Virender Pratap Singh[1,2,*], Rohit Jasrotia[1,*], Kirti Singha[1] and Rajesh Kumar[1]

[1] School of Physics, Shoolini University, Bajhol, Solan, H.P., India
[2] Govt. Degree College, Nadaun (Hamirpur) HP, India

* **Correspondence:** Email: rohitsinghjasrotia4444@gmail.com, kunwar.virender@gmail.com; Tel: +919625233301.

Abstract: In the present review paper, we have explained the structure of Y-type hexagonal ferrite and various synthesis techniques. This paper also includes structural, electrical, magnetic properties and applications of Y-type hexaferrites and focusses on their use in antenna applications and microwave absorbing characteristic materials. Ferromagnetic nature of hexaferrites cause the induction of magnetisation within the crystal structure, which divide them into two groups: First with easy axis of magnetisation is known as uniaxial hexaferrites and second is known as ferroxplana having easy plane of magnetisation. The excellent magnetic properties of Y-type ferrites make them useful in the devices operating at high frequency range. The persistence of high refractive index upto 1 GHz enables these hexagonal ferrites useful in UHF antenna designs with small dimensions. The doping in Y-type hexaferrites affect all the properties. Current developments in Y-type hexaferrites will be explained in detail in the review of literature related to Y-type hexaferrites for the last 25 years, i.e. from 1994 to 2019 in this review paper.

Keywords: Y-type hexaferrite; structural properties; applications of ferrites; microwave absorbing properties and antenna applications

Abbreviations: μ_r: relative permeability (μ = magnetic permeability); ε_r: relative permittivity; ρ: density, in $g \cdot cm^{-3}$; B: applied magnetic field (flux density), in SI units of T; dB: decibel, a

logarithmic unit; EM: electromagnetic; FMR: ferromagnetic resonance; TEM: transmission electron microscope; Me: metal cation; M_r: remnant magnetisation; M_s: saturation magnetisation; MW: microwave Oe: oersted, CGS unit of magnetic strength; SEM: Scanning electron microscope; TEM: Transmission electron microscope; H: magnetic field strength, SI unit is Am^{-1}; H_c: coercivity; VSM: vibrating sample magnetometer; XRD: X-ray diffraction; Y: $Ba_2Me_2Fe_{12}O_{22}$; UHF: Ultra high frequency.

1. Introduction

An iron-based iron (III) oxide known by magnetite (Fe_3O_4) called ferrites, with combination of divalent cation Me, called Spinel having composition $MeFe_2O_4$. There are different types of hexagonal ferrites which are also famous as hexaferrites have their long journey since their discovery [1,2]. These hexaferrites are: M-type ferrites-Barium ferrite or BaM ($BaFe_{12}O_{19}$), Strontium ferrites or SrM ($SrFe_{12}O_{19}$) and cobalt-titanium substituted M ferrite or $BaFe_{12-2x}Co_xTi_xO_{19}$; X-type ferrites—$Ba_2Me_2Fe_{28}O_{46}$, such as $Ba_2Co_2Fe_{28}O_{46}$ or Co_2X; Y-type ferrites—$Ba_2Me_2Fe_{12}O_{22}$, such as $Ba_2Co_2Fe_{12}O_{22}$ or Co_2Y; Z-type ferrites-$Ba_2Me_2Fe_{24}O_{41}$, such as $Ba_2Co_2Fe_{24}O_{41}$ or Co_2Z. W-type ferrites—$BaMe_2Fe_{16}O_{27}$, such as $BaCo_2Fe_{16}O_{27}$ or Co_2W. U-type ferrites—$Ba_4Me_2Fe_{36}O_{60}$, such as $BaCo_2Fe_{36}O_{60}$ or Co_2U.

With the development of modern electronic technology, creates a great demand for the devices operating in high frequency range, which need the magnetic materials with excellent electromagnetic properties. The spinel ferrites have lower cut-off frequency as compared to the soft magnetic hexagonal ferrites, including Y-type and Z-type hexaferrites as the requirement for low temperature cofired ceramics (LTCC) technology is hard Z-type hexagonal ferrites which can be achieved at high sintering temperature (1300 °C) [3–6]. Hence, Y-type hexagonal ferrites have the best use because they acquire good magnetic properties in hyper frequency range at low sintering temperature (1150 °C) [7–9]. A huge amount of magnetic materials is produced by using these hexaferrites world widely [10]. Recent developments in Y-type hexaferrites are expressed in detail in the review of literature related to Y-type hexaferrites. This review is focused on various types of divalent cation substitution in and its effects on the properties of substituted hexaferrites. The excellent review on EM properties and calculated parameters for the evaluation of materials in antenna applications done by Charalampos A. Stergiou et al. [11]. Trukhanov et al. synthesized aluminium doped barium M-type hexaferrite for reporting the crystal structure and magnetic properties of synthesized specimens. In the present investigation, the atomic and lattice parameters are refined with the help of rietveld software [12]. Trukhanov et al. synthesized barium M-type hexaferrite with Al, In substitutions by solid state reaction technique for controlling the electromagnetic characteristics in these nanohexaferrites. It has been found that the external magnetic fields extensively effect the electromagnetic properties of barium M-type hexaferrites. This will occur due to the increase of magnetocrystalline anisotropy [13]. Y-type hexaferrites belong to a category of soft ferrites having high values of dielectric permittivity along with low values of dielectric losses which make it suitable for the microwave application. Jasrotia et al. reported the dielectric measurements of sol-gel synthesized Cd and In substituted barium M-type nanohexaferrites for microwave devices application in which very high values of dielectric constant at high 30 MHz frequency with minute values of losses have been found. Many more authors and researchers have been taken various steps for improving the magnetic and electric properties of Y-type nanohexaferrites in order to make it

suitable for microwave application such as dielectric permittivity, dielectric losses, saturation magnetization, coercivity, etc. [14]. Trukhanov et al. synthesized Ga^{3+} doped barium M-type hexaferrite by conventional solid-state reaction technique for reporting the microstructural and magnetic properties and in aspect of this, these materials make it suitable for microwave absorption applications [15]. Vinnik et al. prepared titanium doped barium M-type hexaferrite by standard solid-state sintering method for investigating the microstructural, electrical and magnetic studies. The rietveld refinement of prepared specimens indicates the preference of Ti^{3+} ions at the interstitial sites of the hexagonal structure. In addition to this, the dc resistivity of all the specimens shows an increasing trend whereas the ac conductivity indicates an inverse phenomenon in aspect of increase in dc resistivity making it suitable for microwave absorption application [16]. The microwave-absorbing materials must have large electric and magnetic loss in a certain frequency range and the microwave absorbing characteristics are influenced by the complex values of permeability and permittivity. Also, the special EM features of ferrites may satisfy the condition of miniaturization in antenna technology without affecting the performance of the antenna. The matching of permeability (μ) and permittivity (ε) values in large possible frequency range and sufficiently low dielectric and magnetic losses are the basic needs to enhance the efficiency of antenna by reducing its size [17–23]. Moreover, some researchers are also working in improving the polarization and multiferroic properties of metal doped M-type hexaferrites. Trukhanov et al. reported the microstructural and multiferroic properties of aluminium doped barium M-type nanohexaferrites. In the present research work, they reported about the spontaneous polarization and co-relation between the magnetic and dielectric environments in which the magnetoelectric effect was found to be increasing along with the increase in Al content [24]. Trukhanov et al. reported the polarization origin and iron positions in the hexagonal crystal structure of indium doped barium M-type hexaferrite. It has been found that the z-component of spontaneous polarization has been found due to the Fe^{3+} and In^{3+} cations displacement at the Fe5-12k position towards the oxygen ion and non-zero dipole moment [25]. The main aim of this review paper is to provide a detailed study on the synthesis of Y-type hexaferrite by different techniques such as sol-gel, co-precipitation, citrate precursor, hydrothermal and many more. In addition, we are also reporting about the microstructural, electric and magnetic characteristics of Y-type hexaferrite for Antenna and Microwave absorbing applications.

2. The discovery, composition and characteristics of Y-type hexagonal ferrites

The hexagonal crystal structure was found in 1938 having composition $PbFe_{7.5}Mn_{3.5}Al_{0.5}Ti_{0.5}O_{19}$ [26]. The compound BaM was confirmed in 1936 with a melting point of 1390 °C [27]. Y-type hexaferrites with formula $Ba_2Me_2Fe_{12}O_{22}$ were discovered firstly, further first two Zn_2Y and Co_2Y with molecular mass 1410 g and density equal to 5.40 $g \cdot cm^{-3}$ with planar magnetic anisotropy were discovered at room temperature. They ferrites with a preferred plane of magnetisation perpendicular to the c-axis at room temperature are called ferroxplana but Cu_2Y hexaferrite has a preferred uniaxial direction of magnetisation. Oxygen excess and deficit can increase and decrease the oxidation degree of 3d-metalls. The changing of charge state of 3d-metalls as a consequence of changing of oxygen content changes such magnetic parameters as Curie point and spontaneous magnetic moment and such electrical parameters as resistivity and band gap. An increase in the unit cell parameter may be also due to oxygen deficiency [28,29]. Moreover, oxygen vacancies effect on exchange interactions. Intensity of exchange interactions decreases with

increasing the oxygen vacancy concentration. In complex oxides there is only indirect exchange. Exchange near the oxygen vacancies is negative according to Goodenough-Kanamori empirical rules. Oxygen vacancies should lead to the formation of a weak magnetic state such as spin glass [30,31]. Jonker in 1956 discovered the hexagonal ferrite $Ba_2Me_2Fe_{12}O_{22}$ (Zn_2Y) [32]. In all hexagonal ferrites, the cobalt substituted barium Y-type hexaferrites possess the highest magnetocrystalline anisotropy. Zn_2Y-type hexagonal ferrites are applicable in microwave devices due to magnetocrystalline planar anisotropy and high permeability. Replacement of Zn ion by divalent ions of Cu^{2+}, Ni^{2+}, Co^{2+}, etc. will change the magnetic properties [33]. By the proper choice of anisotropy field and resonance linewidth, Zn_2Y ferrite can be controlled for suitable applications like microwave device at higher frequencies (>10) GHz [34]. Similarly, at room temperature, addition of Ni^{2+} retains the easy magnetization on the basal plane and weakens the anisotropy. Hexagonal crystal structure with height of the crystal and width of hexagonal plane as shown in Figure 1 [35].

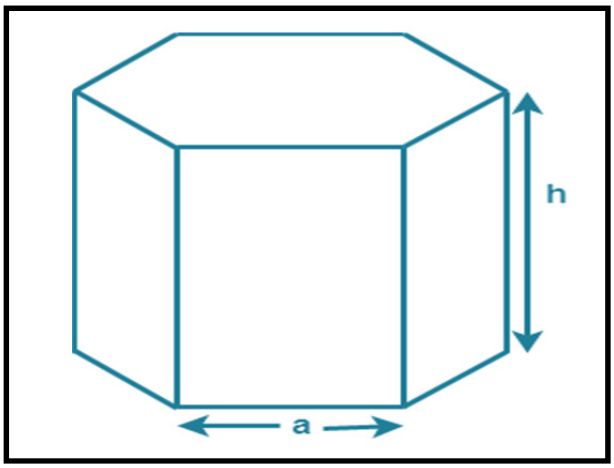

Figure 1. Hexagonal crystal, showing two lattice parameters “a” and “c”.

3. The structure of Y-type hexagonal ferrites

The crystal structure of a ferrite is an interlocked network of positively-charged metal ions (Fe^{3+}, Me^{2+}) and negatively charged divalent oxygen ions (O^{2-}) form. Crystal structure-based classification of ferrites is named as: spinel, garnet, magnetoplumbite or hexaferrite and orthoferrite [23–29]. One-unit cell of spinel with general formula $MeFe_2O_4$, where Me is the divalent metal ion contains 32 octahedral (B) sites, in which trivalent metal ions occupy 16 positions and 64 tetrahedral (A) sites, in which 8 are occupied by divalent metal ions [24,26]. Distribution of the divalent ions on A and B sites further divided spinel ferrites into two types. Garnet ferrite has general formula $R_3Fe_5O_{12}$. It is a polyhedral combination. There exist 16 octahedral, 24 tetrahedral and 16 dodecahedral sites in a unit cell of garnet. One formula unit is distributed as follows: $3M_2O_3$-dodecahedral, $3Fe_3O_3$-tetrahedral and $2Fe_3O_3$-octahedral [30–32]. The spinel ferrite structure and the garnet ferrite are shown in Figure 2a and Figure 2b, respectively [36,37].

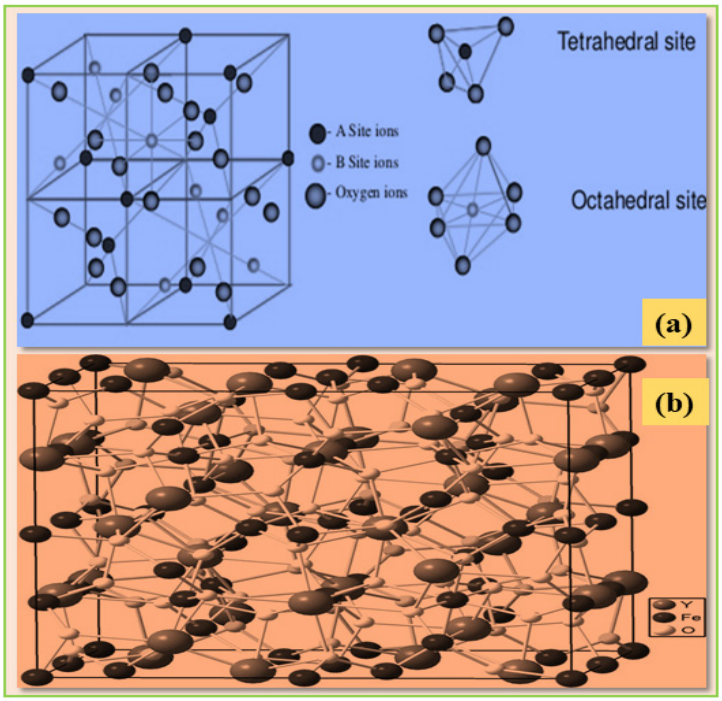

Figure 2. Spinel ferrite (a) and garnet ferrite (b) [36,37].

The divalent and trivalent metal ions are located in the interstitial sites of the structure. Figure 3 shows the compositional diagram of hexagonal ferrites [35]. Types of hexaferrites are listed in Table 1 [36]. All the hexaferrites having highly complex crystal structure are closely related to each other [37] as W ferrite = M + 2S, X ferrite = W + M = 2M + 2S, Z ferrite = M + Y, and U ferrite = Z + M = 2M + Y, where S is Spinel ($MeFe_2O_4$), M is $BaFe_{12}O_{19}$ and Y is $Ba_2Me_2Fe_{12}O_{22}$ by Sudakar et al. [38]. The crystal structure of the M-type hexaferrites may be described by two space groups. One of them is classical P63/mmc (No. 194) space group. Second of them is P63mc (No. 186) space group. Second space group has been used for describing of crystal structure to explain the existence of non-zero spontaneous polarization. This is a polar no centrosymmetric space group [38,39]**.** Four Miller Indices h, j, k, l is essential to describe hexagonal crystal. Two lattice parameters, c (length) and a (width) are required to define the dimensions of the crystal [40]. Y-type hexagonal ferrites have molecular formula $Ba_2Co_2Fe_{12}O_{22}$ with preferred plane of magnetization normal to c-axis. They contain only B_2 layer in which two B_2 layers are sandwiched between four Spinel layers means $Y_6 = B_2S_4$. B_2 layer is shown in Figure 4 [40]. B_2 layer is equivalent to two hexagonal close-packed layers between two spinel plates and in each layer one oxygen atom is replaced by one barium atom. The barium atom of one layer is in contact with three oxygen atoms of other layer and octahedral sites lying in between the oxygen atoms are occupied by small metal ions.

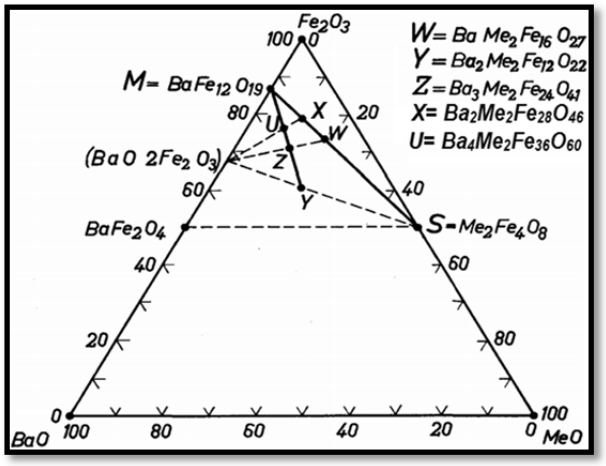

Figure 3. Ternary diagram showing the composition of the main barium hexaferrites [33].

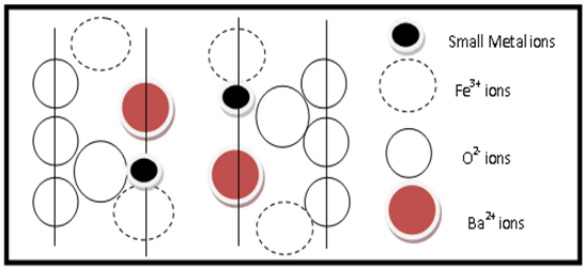

Figure 4. Cross sectional view of the B_2 layer [40].

Table 1. Types of hexagonal ferrites according to structural stacking of blocks.

Symbol	Composition	Crystallographic arrangement	No. of molecules/unit cell	c (A^0)
M	$BaFe_{12}O_{19}$	RSR^*S^* (MM^*)	2M	23.2
U	$Ba_4Me_2Fe_{36}O_{60}$	MM^*Y^*	MeU	38.1
W	$BaMe_2F1_{36}O_{27}$	MSM^*S^*	2MeW	32.8
X	$Ba_2Me_2Fe_{28}O_{46}$	MM^*S	3MeX	84.0
Y	$Ba_2Me_2Fe_{12}O_{22}$	3ST	3MeY	43.5
Z	$Ba_3Me_2Fe_{24}O_{41}$	MYMY	2MeZ	52.3

Y-type is the member of space group R3m consisting of three ST blocks with total of six layers consisting of total 10 octahedral and 4 tetrahedral sites (S block = 4 octahedral + 2 tetrahedral and T block = 6 octahedral + 2 tetrahedral) having c = 43.56 Å in one molecular unit [40]. M-type ferrite structure in cross sectional view looks like as in Figure 5 [41]. S block has composition of either $[Me^{2+}Fe_4^{3+}O_8]^0(S^0)$ or $[Fe_6^{3+}O_8]^{2+}(S^{2+})$, each layer of which consists of four oxygen atoms with three metal atoms, the cation is surrounded by four O^{2-} ions in two tetrahedral sites and by six O^{2-} ions in four octahedral sites. In one S block, there are two-unit cells of spinel with four octahedral and two tetrahedral sites. R block comprise of three hexagonally packed layers with four oxygen atoms in each layer, in which one oxygen atom in the central layer is replaced by barium atom of same size resulting in unit compositional formula $[Me^{2+}Fe_6^{3+}O_{11}]^{2-}$ or $BaFe_6O_{11}$ and it is similar to M_5 unit formed by removing top and bottom layers. In R block, on adding Ba atom, four octahedral and two

tetrahedral sites are replaced by five octahedral sites and no tetrahedral site and a new trigonal bipyramidal site is created surrounded by five oxygen anions. This is a unique position found in R block. In T block, there are four oxygen layers, replacing oxygen in middle two layers by barium atoms and is similar to Y_6 by removing top and bottom layers. Unit formula for T block is $Ba_2Fe_8O_{14}$ and has composition $[Ba_2^{2+}Fe_8^{3+}O_{14}]$ [42–44,9]. The repulsion in two Ba^{2+} ions reduces the five-coordinate trigonal bipyramidal sites to four-coordinate tetragonal sites resulting in two tetrahedral and six octahedral sites, i.e., a total of eight sites. S, R and T block structures are as shown in Figure 6 [41].

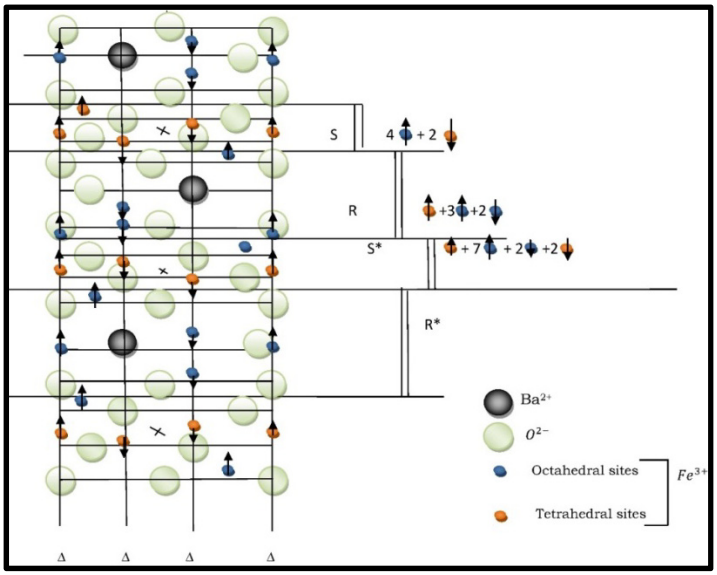

Figure 5. Cross section view of M-type hexaferrite in which vertical lines are axis of threefold symmetry [41].

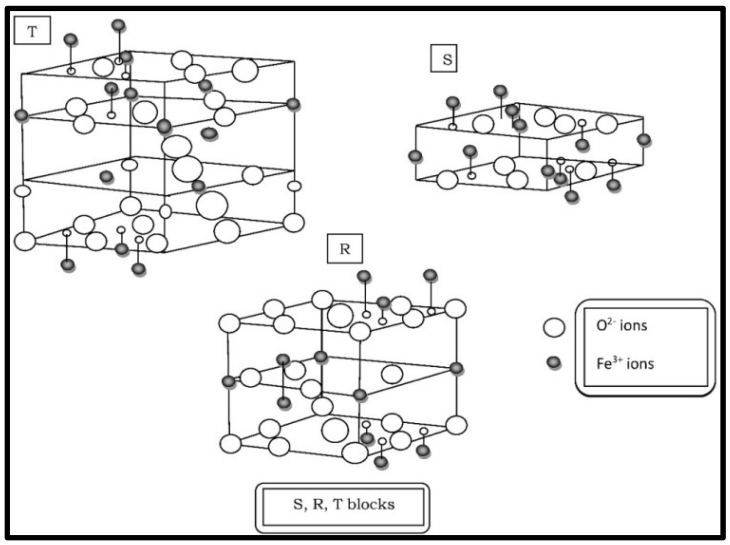

Figure 6. Perspective view of (a) S block, (b) T block, and (c) R block [41].

4. The synthesis methods of Y-type hexagonal ferrites

Y-type hexagonal ferrites are synthesized by different methods like coprecipitation, salt-melt, ion exchange, sol-gel, citrate, hydrothermal, combustion, microemulsions, etc. [45–49]. In spite of these synthesis methods, there are other combined synthesis techniques such as sol gel-citrate method, sol gel-hydrothermal technique and many more. Many researchers use these types of combined methods for synthesizing the hexagonal ferrites. Almessiere et al. synthesized $Sr_{0.3}Ba_{0.4}Pb_{0.3}Fe_{12}O_{19}/CuFe_2O_4$ (x = 2, 3, 4, 5) nanoferrites with the usage of combined citrate-sol gel technique for reporting the co-relation between the chemical composition and electrodynamics characteristics [50]. Kozlovskiy et al. synthesized $Ce(FeTi)O_x$ perovskite ferrite with the usage of combined solid-phase technique for reporting the microstructural and magnetic characteristics of prepared specimens [51]. The physical properties of hexaferrites are influenced significantly by the processing techniques which have further great impact on magnetic properties. The block diagram of synthesis methods of nanomaterials is shown in Figure 7. In this review paper, some of the chemical methods are discussed as shown in Figure 8.

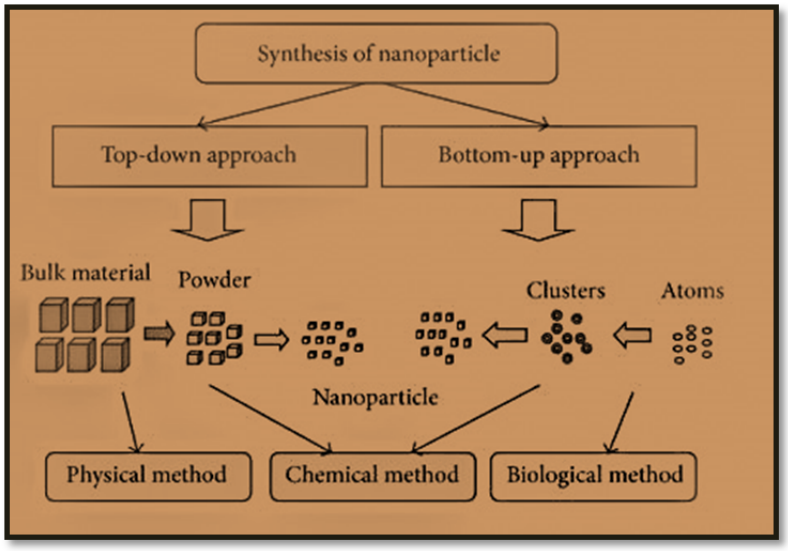

Figure 7. The scheme of synthesis methods of nanoparticles.

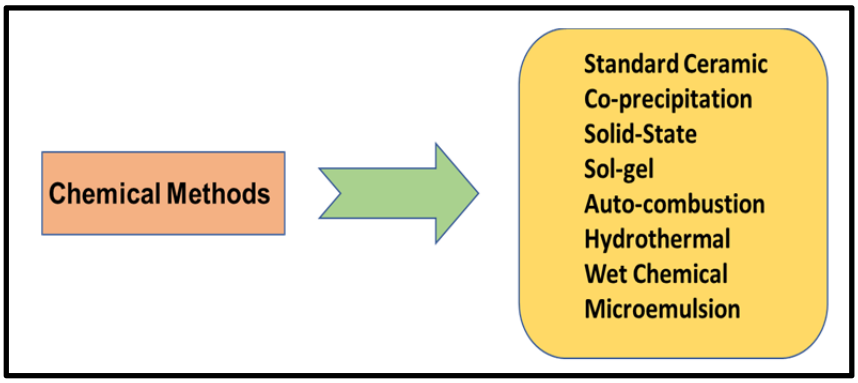

Figure 8. Chemical methods.

4.1. Standard ceramic

In this method, a mixture of barium carbonate powders and oxides is heated to synthesize the hexagonal ferrites. The ceramic powder is then milled to get the finer material. We can get the nanosize after long milling. The single-phase ferrites formation is not possible by this method. Picking of impurity or material loss occur during the processing. High temperature and long duration are required for processing due to low reactivity of the starting materials [52]. To convert ferrites into ultrafine nano agglomerates, "allows nanoparticles to participate in the thermal motion and provides for the possibility of their self-assembly into superstructures by eventually finding the thermodynamic optimum [53].

4.2. Solid state reaction

This method involves the mixing of hydroxide, oxide, carbonate, or sulphate raw materials treated on higher temperature at about 1100 °C for a long duration which yield inhomogeneous microstructures, abnormal grain growth, poor sintering behaviour, and uncontrolled cation stoichiometry [54]. In this method, a mixture of barium carbonate and iron oxide is fired at very high temperatures (1150–1250 °C). The resulting powder is then grounded which can cause impurities in powder and stains in crystal lattices and can affect the magnetic properties [55,34].

4.3. Coprecipitation

The chemical coprecipitation of salts is done with base (NaOH). This method is being used since early 1960s [56,57]. Magnetic stirring and heating at about 70 °C are done. Then particles are washed with deionized water by centrifugation. At the last particles are dried. The schematic chart is shown in Figure 9.

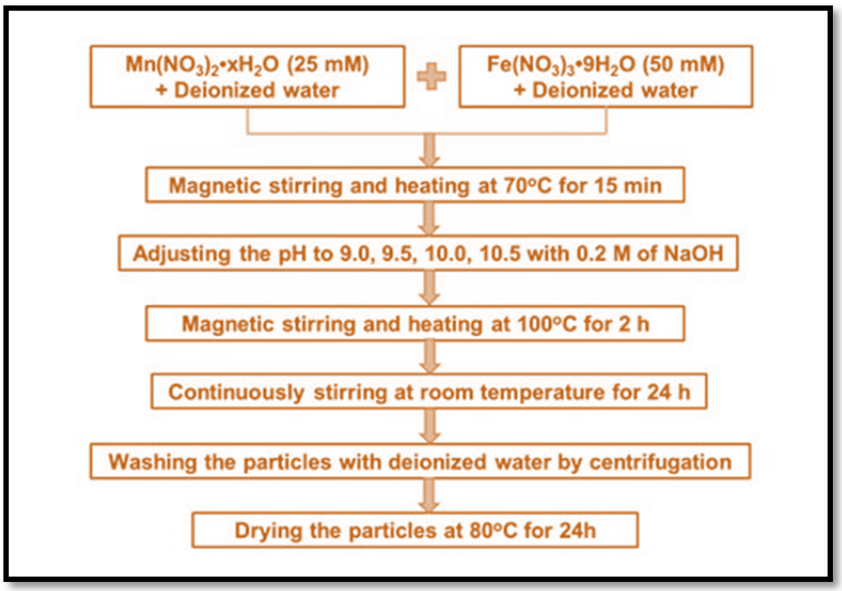

Figure 9. Co-precipitation method.

4.4. Sol-gel

In sol-gel synthesis, homogeneous solution of metal salts is made and poured in the solution of citric acid. An organic coordinating agent ethylene glycol is added to the solution to produce a sol which forms a gel structure upon evaporation of the water. pH is maintained by adding ammonia solution. This method is used to make more complex hexaferrites at nano scale [58]. Sol-gel technique have number of advantages such as low annealing temperature and excellent ability for controlling microstructure [59]. Flow sheet of this method is shown in Figure 10.

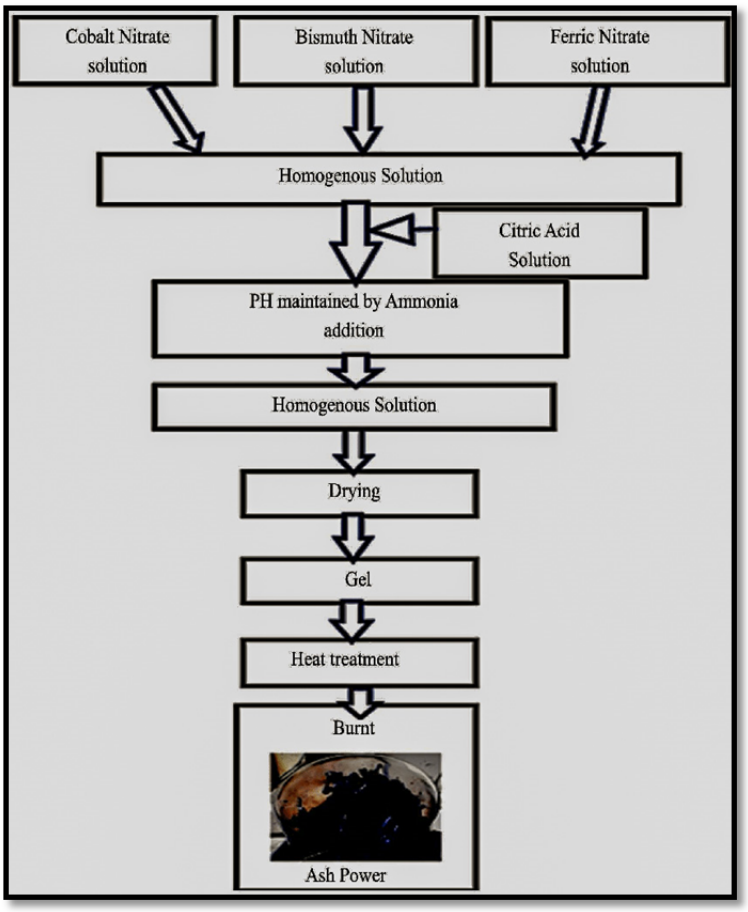

Figure 10. Sol-gel technique.

4.5. Combustion

The solution of salts, ammonia and citric acid along with setting the pH equal to 7 is then evaporated to a dry powder on a hot plate. The citric acid get polymerised and evolved carbon dioxide and cations are completely converted into iron oxide and barium carbonate. The material so obtained possess poor magnetic properties because of small grain size [60]. This process can either proceed via aqueous combustion synthesis (ACS) or via low temperature combustion synthesis (LCS) [61]. The mixture is then auto combusted in microwave oven to get nano powder [62]. The scheme is shown in Figure 11.

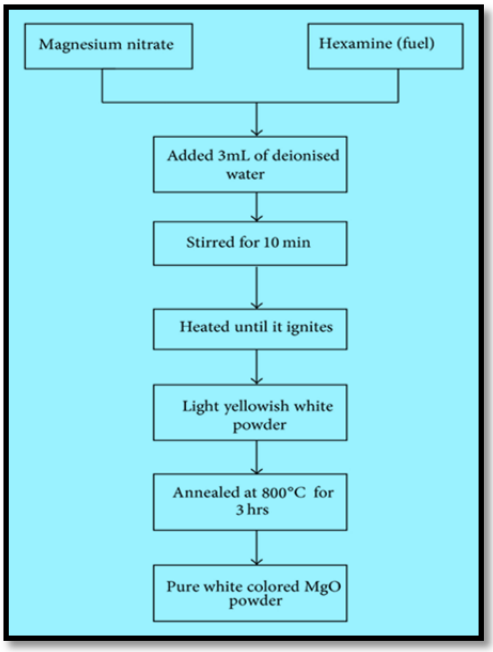

Figure 11. The scheme of combustion method.

4.6. Hydrothermal

In hydrothermal synthesis a solution of metal salts and base are made under pressure to give the product. The unreactive precursors are washed away with dilute HCl. Ataie et al. studied the effects of many bases such as NaOH, KOH and NH_4OH in the synthesis of hexaferrites [63]. Figure 12 is showing the scheme of this method.

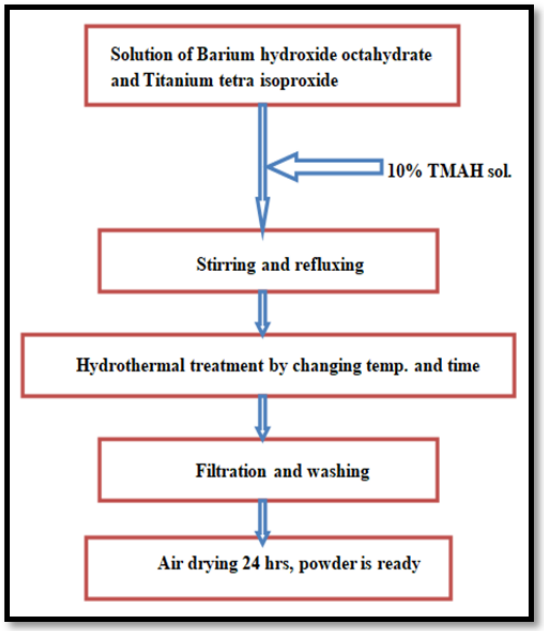

Figure 12. Hydrothermal process.

4.7. Wet chemical

In comparison to ceramic method, wet chemical method is more efficient for the preparation of hexaferrites. In this method, homogeneous mixture is formed of the raw materials. It requires low temperature for processing and long duration for sintering. No material loss occurs during the process. Good thing is that there is greater possibility of single-phase formation [52].

4.8. Microemulsions

Form nanoparticles with mixing of two immiscible liquids stabilized by an artificial film of surface-active agents. Morphology can be controlled in this method [64]. The precipitates are then separated, washed and dried. The method scheme is shown in Figure 13.

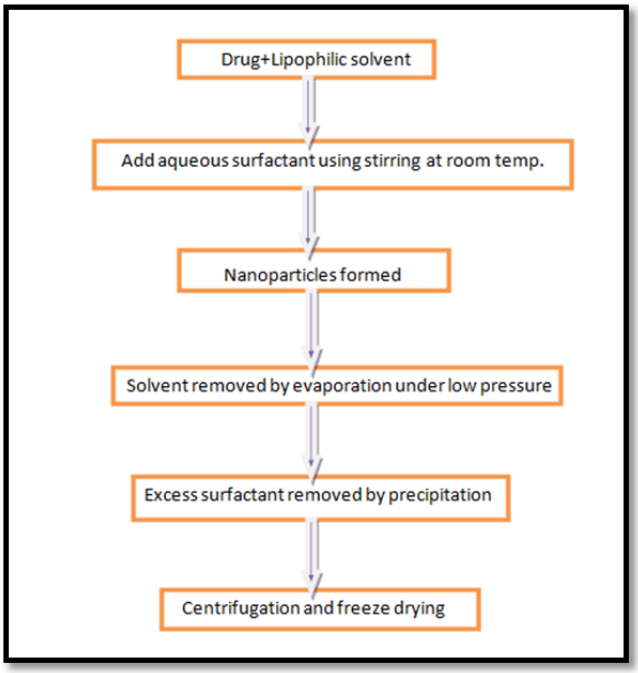

Figure 13. Micro emulsion technique.

5. A review on structural, electrical and magnetic properties of Y-type hexaferrites

Literature related to Y-type hexaferrites was reviewed for the last fifteen years (2005–2019) and enlisted the structural, electrical and magnetic studies in tabular form studied by different researchers with different compositions fabricated with different techniques.

5.1. Structural properties

In the structural properties, we analyse lattice parameters (c and a), cell volume (V), crystal size (D), bulk density, X-ray density and porosity from XRD patterns. And calculate lattice parameters (c and a), cell volume (V), crystal size (D) by using the Eqs 1, 2, and 3 respectively given below [65]:

$$\sin^2\theta = \frac{\lambda^2}{3a^2}(h^2 + hk + k^2) + (\frac{\lambda^2}{4c^2})l^2 \quad (1)$$

Here "λ" is the wavelength, a and c are the lattice constants and h, k, l are the corresponding indices.

$$V = a^2 c \sin 120^0 \quad (2)$$

The crystalline size (D) is calculated from XRD patterns by using well-known Scherrer formula

$$D = \frac{k\lambda}{\beta\cos\theta} \quad (3)$$

where "λ" is the wavelength of the Cu-Kα source (1.5418 A°), "β" is the full width at half maxima, "θ" is the Bragg's angle and "k" is the shape factor (0.89) for hexagonal ferrite-based nanomaterials system. The crystallite size plays an important role in affecting the electromagnetic properties of Y-type hexaferrites. There are actually three parameters such as permittivity (∈), permeability (μ) and conductivity (σ) which are quantified for describing the effect of nanohexaferrite in calculating an electromagnetic quantity in regards with a source. With the decreasing crystallite size of synthesized Y-type nanohexaferrites, the value of permittivity as well as permeability shows an anomalous behaviour whereas the conductivity as well as dielectric loss tangent (tanδ) decreases as a function of crystallites size. The crystallite size of transition metal oxides also influenced the magnetization and curie point i.e. with the decrease in crystallite size, the saturation magnetization (M_s) of prepared samples were found to be decreasing as they are inversely proportional to each other. In addition to this, the average crystallite size distribution also critically affects the electromagnetic characteristics in the region of several GHz through the resonance of domain walls [66].

The X-ray density (d_x), bulk density (d_b) and porosity (P) are calculated by the Eqs 4, 5 and 6, respectively:

$$d_{x-ray} = \frac{ZM}{N_A V_{cell}} \quad (4)$$

$$d_b = \frac{m}{\pi r^2 h} \quad (5)$$

$$P = 1 - \frac{d_b}{d_x} \quad (6)$$

where M is the molar mass, m is the mass and r are the radius and h are the thickness of the pellet, N_A is the Avogadro's number, Z = 3 is the number of molecules per unit cell. Microstructure is imaged with the help of FESEM and HRTEM techniques. This structural study was confirmed with the usage of Raman spectroscopic analysis as reported in Ba–Nd–Cd–In and Mg–Ag–Mn hexagonal and spinel ferrite by Jasrotia et al, (2020) [67]. The structural parameters of the literature reviewed are listed in Table 2.

Table 2. Observed values of structural parameters.

Sr. No.	Composition	a (Å)	c (Å)	Density	D (nm)	Refs.
1.	$Ba_2Zn_{1.2-x}Co_xCu_{0.8}Fe_{12}O_{22}$ (x = 0.0–1.2)	5.875–5.865	43.689–43.506	-	-	[68]
2.	$Ba_2Cd_2(Zr\ Co)_xFe_{12-2x}O_{22}$ (x = 0.0–1.0)	5.88–5.98	43.61–44.14	-	59–46	[69]
3.	$Sr_2Ni_2Fe_{12-y}Cr_yO_{22}$ (y = 0.0–1.5)	5.88–5.90	43.48–43.36	5.03–4.99	44–14	[70]
4.	$Sr_2Me_2Fe_{11}(SnCo)_{0.5}O_{22}$ (Me–Cu and Zn)	5.85 5.90	43.69 43.50	2.85 3.72	8.7–11	[71]
5.	$Ba_2Co_{2-x-y}Zn_xCu_yFe_{12}O_{22}$ (x = 0–2, y = 0–0.8)	5.862–5.870	43.518–43.520	5.12–5.20	-	[72]
6.	$Sr_2Cu_{2-x}Co_xFe_{12}O_{22}$ (x = 0.0–1.0)	5.88–6.45	43.52–43.62	-	-	[73]
7.	$Sr_2Ni_{2-x}Mg_xFe_{12}O_{22}$ (x = 0.0–0.5)	5.88–5.91	43.45–43.15	4.71–3.48	-	[74]
8.	$Sr_2MnNiFe_{12}O_{22b} + xY_2O_3$ (x = 0–5)	5.90–5.88	43.49–43.50	-	22–70	[75]
9.	$Sr_2Ni_xCo_{2-x}Eu_yFe_{12}O_{22}$ (x = 0–1, y = 0–0.1)	c/a=7.37–7.30	-	4.92–4.69	-	[76]
10.	$Sr_2MnNiFe_{12}O_{22}$	5.908	43.155	-	29	[77]
11.	$Ba_2Zn_2Tb_xFe12–xO_{22}$ (x = 0.0–0.1)	5.85–5.91	43.45–44.31	-	20–36	[78]
12.	$Ba_2Co_2Fe_{12}O_{22}$	5.86	43.52	-	-	[79]
	$Ba_2CoCrFe_{12}O_{22}$	5.86	43.49	-	-	
	$Ba_2Co_2Fe_{11}GaO_{22}$	5.86	43.49	-	-	
	$Ba_2CoMgFe_{11}GaO_{22}$	5.89	43.49	-	-	
13.	$Sr_2Co_2Fe_{12-x/2}Al_{y/2}O_{22}$ (y = 0.0–3.0)	5.848–5.821	43.507–43.509	-	-	[80]
14.	$Sr_2Ni_2Al_{x/2}Cr_{x/2}Fe_{12-x}O_{22}$ (x = 0.0–3.0)	5.858–5.875	43.304–43.423	-	-	[81]
15.	$Sr_2Ni_{2-x}Co_xFe_{12}O_{22}$ (x = 0.5)	5.8979	44.45	-	-	[82]
16.	$Sr_2Co_2Ni_xTi_xFe_{12-2x}O_{22}$ (x = 0.0–0.5)	5.89–5.95	43.59–43.69	5.04–4.95	5–45	[83]
17.	$Sr_2Co_2Mn_xPr_xFe_{12-x}O_{22}$ (x = 0.0–0.1)	5.89–5.96	43.35–43.44	5.04–4.89	60–26	[84]

5.2. Electrical properties

In the electrical properties, we calculate dc resistivity (ρ_{dc}) from V-I characteristics of the pellets made of the synthesized samples. Resistivity is calculated by using Eq 7 and the variation of electrical resistivity with temperature follows Eq 8. Other parameters like activation energy (E_a) is calculated from 1000/T vs dc resistivity plots by getting slopes of two regions, one is ferromagnetic region (below Curie temperature) and other is paramagnetic region (above Curie temperature) and Eq 9 is used to calculate the activation energy. Drift mobility (μ_{dc}) at different temperatures is calculated by using the relation given in Eq 10 [70]:

$$\rho = \frac{RA}{h} \tag{7}$$

where ρ is the resistivity, R is resistance, A is area and h is thickness of the pellet.

$$\rho = \rho_0 \exp\left(\frac{E_a}{k_B T}\right) \tag{8}$$

where ρ is the dc electrical resistivity at temperature T, ρ_0 is the resistivity at1/T = 0, E_a is the activation energy and k_B is the Boltzmann's constant.

$$E_a = 8.6 \times 10^{-5} \times \text{slope} \quad (9)$$

$$\mu_d = \frac{1}{ne\rho_{dc}} = \frac{\sigma_{dc}}{ne} \quad (10)$$

where σ_{dc} is the electrical conductivity, e is the charge of electron, n is the concentration of charge carriers and can be calculated from the well-known Eq 11:

$$n = \frac{N_A d_b N_{Fe}}{M} \quad (11)$$

where N_{Fe} is the number of iron atoms and M is the molecular weight of the samples. Some calculated electrical parameter values are listed in Table 3. In Table 3, we are studying the effect of various substitutions on the electrical properties of Y-type hexaferrites such as resistivity, activation energy and drift mobility. It was observed that the change in these parameters depends on the type of substituents. Moreover, with the substitution of rare earth and transition elements, room temperature dc resistivity was found to be increasing whereas drift mobility decreases. The change in electrical resistivity can be explained due to influence of cationic distribution at the specific interstitial sites i.e. Tetrahedral and octahedral. The activation energy is showing the same trend as that of resistivity. In contrast to other complex iron oxides, i.e. perovskites and spinels, the real part of the dielectric constant for the doped M-type hexaferrites decreases more slowly at low frequencies and almost monotonically with diamagnetic substitution. In addition to this, the real and imaginary parts of the permeability have a peak near 50 GHz, which is determined by the level of diamagnetic substitution. The increase of the resonant frequency approximately to 1.5 GHz at the 1 KOe bias field is observed since the internal anisotropy field increases [85,86].

Table 3. Electrical parameters.

Sr. No	Composition	ρ (ohm-cm)	E_a (eV)	μ_d ($cm^2 \cdot v^{-1} \cdot s^{-1}$)	Refs.
1.	$Ba_2Cd_2(ZrCo)_xFe_{12-2x}O_{22}$ (x = 0.0–1.0)	1.47×10^8–3.25×10^8	0.45–0.52	2.54×10^{-13}–1.11×10^{-13}	[69]
2.	$Sr_2Ni_2Fe_{12-y}Cr_yO_{22}$ (y = 0.0–1.5)	60.6×10^8–1.5×10^8	-	0.68×10^{-13}–0.13×10^{-13}	[70]
3.	$Sr_2Mn_xCo_{2-x}Tb_yFe_{12}O_{22}$ (x = 0–1, y = 0–0.1)	0.12×10^8–0.15×10^{10}	-	3.3×10^{-12}–2.5×10^{-15}	[87]
4.	$Sr_2Ni_{2-x}Mg_xFe_{12}O_{22}$ (x = 0.0–0.5)	6.09×10^6–7.52×10^6	0.35–0.50	-	[74]
5.	$Sr_2Ni_xCo_{2-x}Eu_yFe_{12}O_{22}$ (x = 0–1, y = 0–0.1)	1.23×10^6–3.07×10^9	0.16–0.22	-	[76]
6.	$Sr_2MnNiFe_{12}O_{22}$	1.01×10^5	-	-	[77]
7.	$Ba_2Zn_2Tb_xFe12-xO_{22}$ (x = 0.0–0.1)	1.47×10^8–3.25×10^8	0.26–0.39	-	[78]
8.	$Ba_{1.5}Sr_{0.5}CoZnFe_{12-x}Al_xO_{22}$ (x = 0–1)	4.72×10^7–30.34×10^7	-	-	[88]
9.	$Sr_2Co_2Ni_xTi_xFe_{12-x}O_{22}$ (x = 0.0–0.5)	1.8×10^6–4.9×10^9	0.17–0.44	-	[83]
10.	$Sr_2Co_2Mn_xPr_xFe_{12-x}O_{22}$ (x = 0.0–0.1)	2.86×10^7–7.47×10^7	-	-	[84]

5.3. Magnetic properties

Most of the hexaferrites have axis of magnetization along c-axis. The large size of metal ion is responsible for the magnetocrystalline anisotropy in hexaferrites. In magnetic studies, we calculate coercivity (H_c), magnetic saturation (M_s), remanence (M_r), squareness ratio (S) are calculated from M–H loops and magnetic moment (n_B) by using the following Eq 12:

$$n_B = \frac{M_w M_s}{5585} \tag{12}$$

As Y-type hexaferrites are made up of S and T blocks, so S block consists of four octahedral and two opposing tetrahedral magnetic moments, a net of two moments whereas T block consists of six octahedral and two tetrahedral moments out of which two octahedral moments are aligned with the tetrahedral, giving a net of zero moment [27].

S block = 4↑ octahedral and 2↓ tetrahedral = 2↑

T block = 4↑ 2↓ octahedral + 2↓ tetrahedral = 0

Y = 8↑ 2↓ octahedral + 4↓ tetrahedral = 2↑

The opposing spins of T block in Y-type hexaferrites cause low values of magnetic saturation as compared to other hexaferrites and coercivity is the main characteristic to make them useful in potential applications. It depends upon particle size which further depends upon the preparation techniques [89]. The magnetic properties depend on the nature of substitution and their preference to specific interstitial sites such as tetrahedral and octahedral. If the substituents prefer to occupy tetrahedral site (A-site), then the saturation magnetization (M_s) is supposed to enhance whereas if the substituents prefer to occupy octahedral site (B-site), then saturation magnetization (M_s) is supposed to decline but there can be some exceptions. The super exchange interactions also play a critical role in deciding the magnetic properties of Y-type hexaferrite [90,91]. The magnetic parameters of the reviewed literature are listed in Table 4.

Table 4. Magnetic parameters.

Sr. No.	Composition	H_c (Oe)	M_s (emu/g)	M_r (emu/g)	$S = M_r/M_s$	n_B (μ_B)	Refs.
1.	$Ba_2Zn_{1.2-x}Co_xCu_{0.8}Fe_{12}O_{22}$ (x = 0.0–1.2)	48.99–204.22	33.84–27.19	3.81–9.03	0.11–0.12	-	[92]
2.	$Sr_2Me_2Fe_{11}(SnCo)_{0.5}O_{22}$ (Me–Cu and Zn)	Zn-769 Cu-1210	13.44–25.45	5.2–13.3	0.39–0.52	-	[71]
3.	$Sr_2Cu_{2-x}Co_xFe_{12}O_{22}$ (x = 0.0–1.0)	-	60.10–18.03	27.50–8.90	0.46–0.49	-	[73]
4.	$Sr_2Ni_{2-x}Mg_xFe_{12}O_{22}$ (x = 0.0–0.5)	555.44–276.06	40.34–32.84	16.68–10.65	0.41–0.32	9.94–7.63	[74]
5.	$Sr_2Mn_xCo_{2-x}Tb_yFe_{12}O_{22}$ (x = 0–1, y = 0–0.1)	-	77.11–16.95	-	0.41–0.65	15.27–3.68	[87]
6.	$Sr_2Ni_2Fe_{12}O_{22}$	945–207	49.4–52.6	23.9–15.6	0.48–0.30	-	[93]
7.	$Ba_2Co_2Fe_{12}O_{22}$ $Ba_2CoCrFe_{12}O_{22}$	123 23	33.9 37.5	7.90 1.58	0.23 0.04	- -	[79]
8.	$Sr_2Ni_2Al_{x/2}Cr_{x/2}Fe_{12-x}O_{22}$ (x = 0.0–3.0)	840–1160	39.61–30.11	17.51–14.62	0.44–0.49	-	[81]

Continued on next page

Sr. No.	Composition	H_c (Oe)	M_s (emu/g)	M_r (emu/g)	$S = M_r/M_s$	n_B (μ_B)	Refs.
9.	$Sr_2Ni_{x/2}Co_{2-x}Mg_{x/2}Fe_{12}O_{22}$ (x = 0–0.6)	1140–250	30–50.06	13.30–10.62	0.44–0.21	-	[94]
10.	$Ba_2Co_{1-x}Zn_xFe_{12}O_{22}$ (x = 0.0–2.0)	255–45	31.1–35.2	14.3–5.0	0.46–0.14	-	[95]
11.	$Sr_2Co_2Mn_xPr_xFe_{12-x}O_{22}$ (x = 0.0–0.1)	549–1630	51.42–18.12	13.5–8	0.26–0.44	-	[84]

6. Y-type hexaferrites hybrid magnetic nanomaterials for antenna applications and microwave absorbing characteristic materials

Know et al. [96] observed two types of resonances, one is at lower frequency due to domain wall resonance and other is at higher frequency due to spin rotational resonance in the microwave absorption characteristic studies of rubber composites. No variation was observed in domain wall resonance with increasing Zn content but the spin rotational resonance was shifted towards lower frequency. It was analysed that only spin rotational resonance influenced the microwave absorbing characteristics not the domain wall resonance. Xu et al. [97] reported composition $Ba_2Co_{1.8}Cu_{0.2}Fe_{12}O_{22}$ (Y-type hexaferrite rod) as high absorbent material. FMR frequency was reported to be tuned by the rod dimension because the use of ferrite rods reduced the weight of microwave absorber instead of ferrite slabs. Stergiou et al. [11] examined the potential of the Y-type hexagonal ferrites $BaSrCo_{2-x}Ni_xFe_{12}O_{22}$ as passive microwave absorbing materials and magneto-dielectric antenna substrates and the composition, microstructure and static characteristics along with EM properties upto range of 18 GHz of the fabricated samples were in conjunction with. It was analysed that Ni^{2+} substitution resulted in the enhancement of permeability and permittivity. The persistence of high refractive index upto 1 GHz enables these hexagonal ferrites useful in UHF antenna designs with small dimensions as given in Table 5.

Table 5. EM properties and calculated parameters for the evaluation of materials in antenna applications.

f	Ni	μ	tan δ_m	ε	tan δ_e	N ($Re\sqrt{\mu * \varepsilon^*}$)	A ($\sqrt{\mu'}/\varepsilon'$)	B ($\tan\delta_m + \tan\delta_e$)	C (A/B)
500 MHz	0	2.1	0.02	16.2	0.25	5.9	0.36	0.27	1.34
	0.5	2.5	0.08	17.8	0.31	6.6	0.37	0.38	0.97
	1.0	2.7	0.13	26.1	0.40	8.4	0.32	0.53	0.60
	1.5	3.2	0.18	26.6	0.42	9.3	0.35	0.59	0.58
	2.0	5.4	0.36	30.0	0.45	12.7	0.42	0.81	0.52
1 GHz	0.5	2.3	0.19	15.9	0.27	6.1	0.38	0.46	0.83
	1.0	2.5	0.27	22.1	0.38	7.4	0.33	0.64	0.52
	1.5	2.7	0.39	22.6	0.38	7.8	0.35	0.77	0.45
	2.0	3.7	0.82	24.9	0.43	9.7	0.39	1.24	0.31

Song et al. [88] examined the electromagnetic and microwave absorbing properties of polycrystalline with composition $Ba_{1.5}Sr_{0.5}CoZnFe_{12-x}Al_xO_{22}$ (x = 0–1) over microwave range. observed the maximum absorption of −19 dB at 11.5 GHz with bandwidth (RL < −10 dB) more than at 6 GHz for x = 0.3. Liu et al. [98] studied the microwave absorbing properties of sol-gel synthesized strontium ferrites and sintered them at 1200 °C temperature for different holding time (2h, 4h, 6h, 8h) and observed a shift in the absorption frequency peak of ferrites towards low-

frequency region with increase in holding time. It was concluded that the ferrite holding at temperature 1200 °C for 4 h had the best microwave absorbing property as shown in Figure.

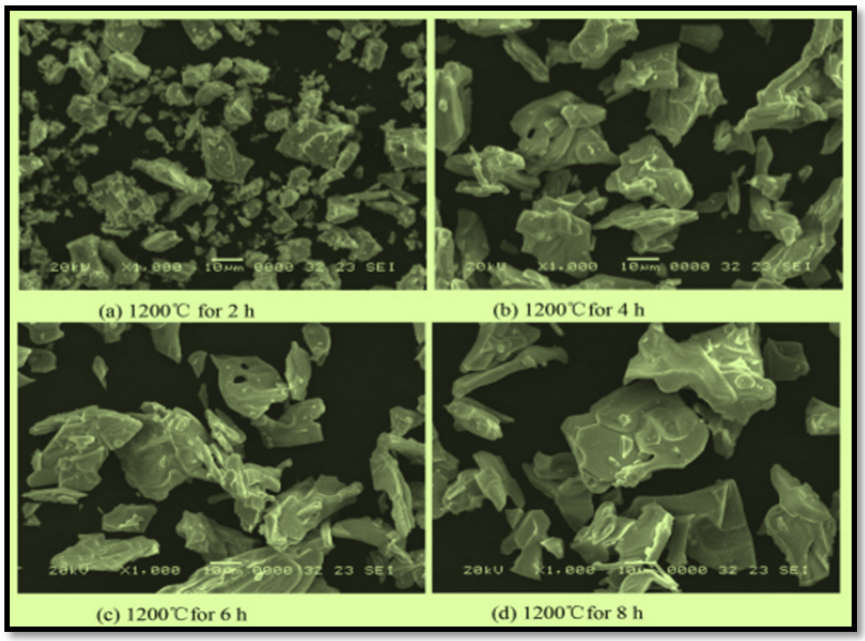

Figure 14. SEM images at temperature of 1200 °C at different time duration [98].

Although except antenna and microwave absorbing applications, there are many other applications of hexaferrites e.g. in information storage, motors, generators, transformers, sensors, mobile communications, transport, security, aerospace, defence, medical field and mostly used magnetic materials are ferromagnetic ceramics. In permanent magnets, hard ferrites are used in all applications made up of either as sintered magnets or bonded magnets are cheaper. Although permanent magnets made from of rare earth metal alloys are the best but they are costly to manufacture because of unavailability of raw materials. M-type ferrites have mostly use in it [99]. Hard ferrites have high value of coercivity used in permanent magnets. Barium hexaferrites are applicable in focussing magnets of TV tubes and transformer core. Due to low coercivity, low eddy and dielectric losses, high resistivity, low remanent flux density and high permeability, soft ferrites are used in transformers and inductors. In electrical and microwave devices, mostly use hexagonal ferrites due to high operating frequency, elimination of conductor losses [100], high electrical resistivity and rapid realignment of domains to minimise the energy losses [10]. Currently, large capacity data storage media are required. In storage and recording, low saturation magnetisation and coercivity are required to overwrite the data [101]. In plastoferrites, bonded magnets powder is injected into a resin or thermoplastic matrix and the products so formed are hard to break [94]. In medical field, hexaferrites have many applications in drug targeting, hyperthermia, nuclear magnetic resonance imaging and magnetomotive biomedical implants but toxic nature of barium restricts the use of them in human body [102]. In environmental science, they are used in treating polluted waste water. They have other applications in sensors, catalyst, high density information storage, etc. [103]. The applications of hexaferrites are illustrated in Figure 15.

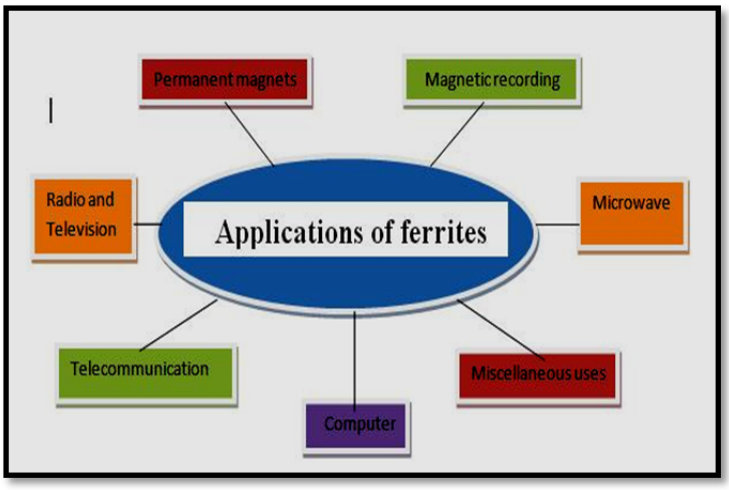

Figure 15. Applications of Y-type hexaferrites.

7. Conclusion

This paper is focused on the historical developments of y-type hexagonal ferrites and their structure, synthesis methods, various types of properties and applications in different fields, especially in antenna applications. In the literature review, we discussed the various types of properties like structural, electrical and magnetic. From the data, a single-phase formation was observed in many doped Y-type hexaferrites with particle size in nano range. SEM and TEM images confirmed the nanosize. Electrical studies revealed the increment in room temperature resistivity and activation energy with the substitution of different types of dopants and decrease in resistivity with rise in temperature is confirming the semiconducting behaviour. Dielectric properties revealed the decrease in dielectric constant, tangent loss factor and dielectric loss with the applied frequency. This increase in resistivity and decrease in dielectric properties make them useful in the microwave devices and the devices operating at higher frequency. Magnetic properties revealed the increase in coercivity make them useful in perpendicular recording media and decrease in coercivity, magnetic moment and magnetic saturation affirm the use of these materials in multilayer chip inductors and beads as high resistivity and low coercivity are basic requirement of these applications. The study of different methods of synthetization of Y-type hexaferrites confirmed that the results of sol-gel technique and wet chemical method are better than other methods. There are many applications in computers, radio and television, telecommunication, medical, filters, chemical reactions, etc.

Acknowledgments

The author would firstly like to thank the editor and reviewers for giving valuable suggestions which helps us in improving our review paper.

Conflicts of interests

There are no conflicts of interest between the authors for publishing this review article.

References

1. Jasrotia R, Singh VP, Sharma RK, et al. (2019) Analysis of effect of Ag^+ ion on microstructure and elemental distribution of strontium W-type hexaferrites. *AIP Conference Proceedings* 2142: 140004.
2. Jasrotia R, Singh VP, Sharma RK, et al. (2019) Analysis of optical and magnetic study of silver substituted SrW hexagonal ferrites. *AIP Conference Proceedings* 2142: 090004.
3. Zhang H, Zhou J, Wang Y, et al. (2002) Microstructure and physical characteristics of novel Z-type hexaferrite with Cu modification. *J Electroceram* 9: 73–79.
4. Zhang H, Zhou J, Wang Y, et al. (2002) Investigation on physical characteristics of novel Z-type $Ba_3Co_{2(0.8–x)}Cu_{0.40}Zn_{2x}Fe_{24}O_{41}$ hexaferrite. *Mater Lett* 56: 397–403.
5. Zhang H, Zhou J, Wang Y, et al. (2002) The effect of Zn ion substitution on electromagnetic properties of low-temperature fired Z-type hexaferrite. *Ceram Int* 28: 917–923.
6. Kračunovska S, Töpfer J (2009) Preparation, thermal stability and permeability behavior of substituted Z-type hexagonal ferrites for multilayer inductors. *J Electroceram* 22: 227–232.
7. Bai Y, Zhou J, Gui Z, et al. (2002) An investigation of the magnetic properties of Co_2Y hexaferrite. *Mater Lett* 57: 807–811.
8. Bai Y, Zhou J, Gui Z, et al. (2002) Magnetic properties of Cu, Zn-modified Co_2Y hexaferrites. *J Magn Magn Mater* 246: 140–144.
9. Bai Y, Zhou J, Gui Z, et al. (2003) Complex Y-type hexagonal ferrites: an ideal material for high-frequency chip magnetic components. *J Magn Magn Mater* 264: 44–49.
10. Özgür Ü, Alivov Y, Morkoç H (2009) Microwave ferrites, part 1: fundamental properties. *J Mater Sci-Mater El* 20: 789–834.
11. Stergiou CA, Litsardakis G (2016) Y-type hexagonal ferrites for microwave absorber and antenna applications. *J Magn Magn Mater* 405: 54–61.
12. Trukhanov AV, Turchenko VO, Bobrikov IA, et al. (2015) Crystal structure and magnetic properties of the $BaFe_{12–x}Al_xO_{19}$ (x = 0.1–1.2) solid solutions. *J Magn Magn Mater* 393: 253–259.
13. Trukhanov AV, Kostishyn VG, Panina LV, et al. (2018) Control of electromagnetic properties in substituted M-type hexagonal ferrites. *J Alloy Compd* 754: 247–256.
14. Jasrotia R, Singh VP, Sharma B, et al. (2020) Sol-gel synthesized Ba–Nd–Cd–In nanohexaferrites for high frequency and microwave devices applications. *J Alloy Compd* 154687.
15. Trukhanov AV, Darwish MA, Panina LV, et al. (2019) Features of crystal and magnetic structure of the $BaFe_{12–x}Ga_xO_{19}$ ($x \leq 2$) in the wide temperature range. *J Alloy Compd* 791: 522–529.
16. Vinnik DA, Zhivulin VE, Starikov AY, et al. (2020) Influence of titanium substitution on structure, magnetic and electric properties of barium hexaferrites $BaFe_{12–x}Ti_xO_{19}$. *J Magn Magn Mater* 498: 166117.
17. Karilainen AO, Ikonen PM, Simovski CR, et al. (2011) Experimental studies on antenna miniaturisation using magneto-dielectric and dielectric materials. *IET Microw Antenna P* 5: 495–502.
18. Souriou D, Mattei JL, Chevalier A, et al. (2010) Influential parameters on electromagnetic properties of nickel-zinc ferrites for antenna miniaturization. *J Appl Phys* 107: 09A518.

19. Lee J, Hong YK, Bae S, et al. (2011) Broadband bluetooth antenna based on Co_2Z hexaferrite-glass composite. *Micro Opt Techn Let* 53: 1222–1225.
20. Mattei J-L, Huitema L, Queffelec P, et al. (2011) Suitability of Ni–Zn ferrites ceramics with controlled porosity as granular substrates for mobile handset miniaturized antennas. *IEEE T Magn* 47: 3720–3723.
21. Lee J, Hong YK, Lee W, et al. (2013) Role of small permeability in gigahertz ferrite antenna performance. *IEEE Magn Lett* 4: 5000104–5000104.
22. Canneva F, Ferrero F, Chevalier A, et al. (2013) Miniature reconfigurable antenna with magneto dielectric substrate for DVB-H band. *Micro Opt Techn Le*t 55: 2007–2011.
23. Mattei JL, Le Guen E, Chevalier A (2015) Dense and half-dense NiZnCo ferrite ceramics: Their respective relevance for antenna downsizing, according to their dielectric and magnetic properties at microwave frequencies. *J Appl Phys* 117: 084904.
24. Trukhanov AV, Trukhanov SV, Kostishin VG, et al. (2017) Multiferroic properties and structural features of M-type Al-substituted barium hexaferrites. *Phys Solid State* 59: 737–745.
25. Trukhanov SV, Trukhanov AV, Turchenko VA, et al. (2018) Polarization origin and iron positions in indium doped barium hexaferrites. *Ceram Int* 44: 290–300.
26. Adelskold V (1938) Crystal structure of lead dodecairon (III) oxide. *Arkiv for Kemi, Mineralogi och Geologi A* 12: 1–9.
27. Arkel A van, Verwey EJW, Bruggen MG (1936) Recueil Tray. chim. *Pays-Bas* 55: 331.
28. Trukhanov SV (2005) Peculiarities of the magnetic state in the system $La_{0.70}Sr_{0.30}MnO_{3-\gamma}$ ($0 \le \gamma \le 0.25$). *J Exp Theor Phys* 100: 95–105.
29. Zdorovets MV, Arbuz A, Kozlovskiy AL (2020) Synthesis of $LiBaZrO_x$ ceramics with a core-shell structure. *Ceram Inter* 46: 6217–6221.
30. Trukhanov SV, Lobanovski LS, Bushinsky MV, et al. (2003) Magnetic phase transitions in the anion-deficient $La_{1-x}Ba_xMnO_{3-x/2}$ ($0 \le x \le 0.50$) manganites. *J Phys-Condense Mat* 15: 1783.
31. Trukhanov SV, Troyanchuk IO, Trukhanov AV, et al. (2006) Concentration-dependent structural transition in the $La_{0.70}Sr_{0.30}MnO_{3-\delta}$ system. *JETP lett* 84: 254–257.
32. Jonker GH, HP Wijn, PB Braun (1956) Ferroxplana, hexagonal ferromagnetic iron-oxide compounds for very high frequencies. *Philips Tech Rev* 18: 145.
33. Albanese G (1977) Recent advances in hexagonal ferrites by the use of nuclear spectroscopic methods. *J Phys Colloq* 38: C1–85.
34. Yu HF, Huang KC (2002) Preparation and characterization of ester-derived $BaFe_{12}O_{19}$ powder. *J Mater Res* 17: 199–203.
35. Jaswon MA (1965) *An Introduction to Mathematical Crystallography*, American: Elsevier.
36. Kaiser M (2009) Effect of nickel substitutions on some properties of Cu–Zn ferrites. *J Alloy Compd* 468: 15–21.
37. Song YY, Ordóñez-Romero CL, Wu M (2009) Millimeter wave notch filters based on ferromagnetic resonance in hexagonal barium ferrites. *Appl Phys Lett* 95: 142506.
38. Turchenko V, Trukhanov A, Trukhanov S, et al. (2019) Correlation of crystalline and magnetic structures of barium ferrites with dual ferroic properties. *J Magn Magn Mater* 477: 9–16.
39. Turchenko V, Kostishyn VG, Trukhanov S, et al. (2020) Crystal and magnetic structures, magnetic and ferroelectric properties of strontium ferrite partially substituted with in ions. *J Alloy Compd* 821: 153412.

40. Braun PB (1957) The crystal structures of a new group of ferromagnetic compounds. *Philips Res Rep* 12: 491–548.
41. Singh VP, Jasrotia R, Kumar R, et al. (2018) A current review on the synthesis and magnetic properties of M-type hexaferrites material. *WJCMP* 8: 36.
42. Sugimoto M (1982) Properties of ferroxplana-type hexagonal ferrites, *Handbook of Ferromagnetic Materials*, Elsevier, 3: 393–440.
43. Novák P, Knížek K, Rusz J (2007) Magnetism in the magnetoelectric hexaferrite system $(Ba_{1-x}Sr_x)_2Zn_2Fe_{12}O_{22}$. *Phys Rev B* 76: 024432.
44. Salunkhe MY, Kulkarni DK (2004) Structural, magnetic and microstructural study of $Sr_2Ni_2Fe_{12}O_{22}$. *J Magn Magn Mater* 279: 64–68.
45. Wiederhorn SM (1969) Fracture surface energy of glass. *J Am Ceram Soc* 52: 99–105.
46. Neckenburger E, Severin H, Vogel JK, et al. (1964) Ferrite hexagonaler Kristallstrustur mit hoher Grenzfrequenz. *Z Angew Phys* 18: 65.
47. Vinnik MA (1965) Phase relationships in the BaO–CoO–Fe_2O_3 system. *Russ J Inorg Chem* 10: 1164–1167.
48. Kuznetsova SI, Naiden EP, Stepanova TN (1988) Topotactic reaction kinetics in the formation of hexagonal ferrite $Ba_3Co_2Fe_{24}O_{41}$. *Inorg Mater* 24: 856–859.
49. Drobek J, Bigelow WC, Wells RG (1961) Electron microscopic studies of growth structures in hexagonal ferrites. *J Am Ceram Soc* 44: 262–264.
50. Almessiere MA, Trukhanov AV, Slimani Y, et al. (2019) Correlation between composition and electrodynamics properties in nanocomposites based on hard/soft ferrimagnetics with strong exchange coupling. *Nanomaterials* 9: 202.
51. Kozlovskiy A, Kenzhina I, Zdorovets M (2019) Synthesis, phase composition and magnetic properties of double perovskites of A $(FeM)O_{4-x}$ type (A = Ce; M = Ti). *Ceram Inter* 45: 8669–8676.
52. Ahmed MA, Okasha N, El-Dek SI (2008) Preparation and characterization of nanometric Mn ferrite via different methods. *Nanotechnology* 19: 065603.
53. Naiden EP, Itin VI, Terekhova OG (2003) Mechanochemical modification of the phase diagrams of hexagonal oxide ferrimagnets. *Tech Phys Lett* 29: 889–891.
54. Dufour J, López-Vidriero E, Negro C, et al. (1998) Improvement of ceramic method for synthesizing M-type hexaferrites. *Chem Eng Commun* 167: 227–244.
55. Tenzer RK (1963) Influence of particle size on the coercive force of barium ferrite powders. *J Appl Phys* 34: 1267–1268.
56. Mee CD, Jeschke JC (1963) Single-domain properties in hexagonal ferrites. *J Appl Phys* 34: 1271–1272.
57. Roos W (1980) Formation of chemically coprecipitated barium ferrite. *J Am Ceram Soc* 63: 601–603.
58. Xiong G, Xu M, Mai Z (2001) Magnetic properties of $Ba_4Co_2Fe_{36}O_{60}$ nanocrystals prepared through a sol-gel method. *Solid State Commun* 118: 53–58.
59. Kour S, Sharma RK, Jasrotia R, et al. (2019) A brief review on the synthesis of maghemite (γ-Fe_2O_3) for medical diagnostic and solar energy applications. *AIP Conference Proceedings*, AIP Publishing, 090007.
60. Mishra SK, Pathak LC, Rao V (1997) Synthesis of submicron Ba-hexaferrite powder by a self-propagating chemical decomposition process. *Mater Lett* 32: 137–141.

61. Hong YS, Ho CM, Hsu HY, et al. (2004) Synthesis of nanocrystalline $Ba(MnTi)_xFe_{12-2x}O_{19}$ powders by the sol-gel combustion method in citrate acid–metal nitrates system (x = 0, 0.5, 1.0, 1.5, 2.0). *J Magn Magn Mater* 279: 401–410.
62. Junliang L, Yanwei Z, Cuijing G, et al. (2010) One-step synthesis of barium hexaferrite nano-powders via microwave-assisted sol-gel auto-combustion. *J Eur Ceram Soc* 30: 993–997.
63. Lalegani Z, Nemati A (2017) Influence of synthesis variables on the properties of barium hexaferrite nanoparticles. *J Mater Sci-Mater El* 28: 4606–4612.
64. Pillai V, Kumar P, Hou MJ, et al. (1995) Preparation of nanoparticles of silver halides, superconductors and magnetic materials using water-in-oil microemulsions as nano-reactors. *Adv Colloid Interfac* 55: 241–269.
65. Jasrotia R, Singh VP, Kumar R, et al. (2019) Analysis of Cd^{2+} and In^{3+} ions doping on microstructure, optical, magnetic and mossbauer spectral properties of sol-gel synthesized BaM hexagonal ferrite based nanomaterials. *Results Phys* 12: 1933–1941.
66. Trukhanov SV, Lobanovski LS, Bushinsky MV, et al. (2005) Study of A-site ordered $PrBaMn_2O_{6-\delta}$ manganite properties depending on the treatment conditions. *J Phys-Condens Mat* 17: 6495.
67. Jasrotia R, Singh VP, Kumar R, et al. (2020) Raman spectra of sol-gel auto-combustion synthesized Mg–Ag–Mn and Ba–Nd–Cd–In ferrite based nanomaterials. *Ceram Int* 46: 618–621.
68. Bai Y, Zhou J, Gui Z, et al. (2006) Phase formation process, microstructure and magnetic properties of Y-type hexagonal ferrite prepared by citrate sol-gel auto-combustion method. *Mater Chem Phys* 98: 66–70.
69. Iqbal MJ, Barkat-ul-Ain (2009) Synthesis and study of physical properties of Zr^{4+}–Co^{2+} co-doped barium hexagonal ferrites. *Materials Science and Engineering B* 164: 6 –11.
70. Iqbal MJ, Liaqat F (2010) Physical and electrical properties of nanosized Mn- and Cr-doped strontium Y-type hexagonal ferrites. *J Am Ceram Soc* 93: 474–480.
71. Badwaik V, Badwaik D, Nanoti V, et al. (2012) Study of some structural and magnetic properties of $Sr_2Me_2Fe_{11}(SnCo)_{0.5}O_{22}$ nanoferrites. *Int J Know Eng* 3: 58–60.
72. Bierlich S, Töpfer J (2012) Zn- and Cu-substituted Co_2Y hexagonal ferrites: sintering behavior and permeability. *J Magn Magn Mater* 324: 1804–1808.
73. Jotania RB, Virk HS (2012) Y-type Hexaferrites: structural, dielectric and magnetic properties, In: Virk HS, Kleemann W, *Solid State Phenomena*, Trans Tech Publications, 189: 209–232.
74. Elahi A, Ahmad M, Ali I, et al. (2013) Preparation and properties of sol-gel synthesized Mg-substituted Ni_2Y hexagonal ferrites. *Ceram Int* 39: 983–990.
75. Irfan M, Islam MU, Ali I, et al. (2014) Effect of Y_2O_3 doping on the electrical transport properties of $Sr_2MnNiFe_{12}O_{22}$ Y-type hexaferrite. *Curr Appl Phys* 14: 112–117.
76. Ali I, Islam MU, Ashiq MN, et al. (2014) Effect of Eu–Ni substitution on electrical and dielectric properties of Co–Sr–Y-type hexagonal ferrite. *Mater Res Bull* 49: 338–344.
77. Aslam A, Islam MU, Ali I, et al. (2014) High frequency electrical transport properties of $CoFe_2O_4$ and $Sr_2NiMnFe_{12}O_{22}$ composite ferrites. *Ceram Int* 40: 155–162.
78. Ali I, Shaheen N, Islam MU, et al. (2014) Study of electrical and dielectric behavior of Tb^+ 3 substituted Y-type hexagonal ferrite. *J Alloy Compd* 617: 863–868.
79. Mahmood SH, Zaqsaw MD, Mohsen OE, et al. (2015) Modification of the magnetic properties of Co_2Y hexaferrites by divalent and trivalent metal substitutions, In: Jotania RB, Virk HS, *Solid State Phenomena*, Trans Tech Publications, 241: 93–125.

80. Nikzad A, Ghasemi A, Tehrani MK, et al. (2015) Y-type strontium hexaferrite: the role of Al substitution, structural, and magnetic consequence. *J Supercond Novel Magn* 28: 3579–3586.
81. Mirzaee O, Mohamady R, Ghasemi A, et al. (2015) Study of the magnetic and structural properties of Al–Cr codoped Y-type hexaferrite prepared via sol-gel auto-combustion method. *Int J Mod Phys B* 29: 1550090.
82. Behare AV, Kumar M, Salunkhe Y, Nandanwar AK (2016) Effect of Sol-gel preparation Technique on the properties of magnetically substituted Y-type hexaferrites. *International Journal of Engineering Development & Research* 4: 2321-9939.
83. Ahmad B, Ashiq MN, Mumtaz S, et al. (2018) Synthesis and electrical behavior of Ni–Ti substituted Y-type hexaferrites for high frequency application. *J Magn Magn Mater* 451: 787–792.
84. Shakeel H, Khan HM, Ali I, et al. (2019) Structural, magnetic and electrical study of rare earth doped Y-type hexaferrites. *J Mater Sci-Mater El* 30: 6708–6717.
85. Trukhanov AV, Almessiere MA, Baykal A, et al. (2019) Influence of the charge ordering and quantum effects in heterovalent substituted hexaferrites on their microwave characteristics. *J Alloy Compd* 788: 1193–1202.
86. Trukhanov AV, Astapovich KA, Almessiere MA, et al. (2020) Pecularities of the magnetic structure and microwave properties in $Ba(Fe_{1-x}Sc_x)_{12}O_{19}$ ($x < 0.1$) hexaferrites. *J Alloy Compd* 822: 153575.
87. Ali I, Islam MU, Ashiq MN, et al. (2014) Role of Tb–Mn substitution on the magnetic properties of Y-type hexaferrites. *J Alloy Compd* 599: 131–138.
88. Song Y, Zheng J, Sun M, et al. (2016) The electromagnetic and microwave absorbing properties of polycrystalline Y-type $Ba_{1.5}Sr_{0.5}CoZnFe_{12-x}Al_xO_{22}$ hexaferrites over the microwave range. *J Mater Sci-Mater El* 27: 4131–4138.
89. Pullar RC (2012) Hexagonal ferrites: a review of the synthesis, properties and applications of hexaferrite ceramics. *Prog Mater Sci* 57: 1191–1334.
90. Jasrotia R, Kumar G, Batoo KM, et al. (2019) Synthesis and characterization of Mg–Ag–Mn nano-ferrites for electromagnet applications. *Physica B* 569: 1–7.
91. Jasrotia R, Singh VP, Kumar R, et al. (2019) Effect of Y^{3+}, Sm^{3+} and Dy^{3+} ions on the microstructure, morphology, optical and magnetic properties NiCoZn magnetic nanoparticles. *Result Phys* 15: 102544.
92. Bai Y, Zhou J, Gui ZL, et al. (2005) Preparation and magnetic properties of Y-type ferroxplana by sol-gel method, In: Pan W, Gong GH, Ge CC, et al., *Key Engineering Materials*, Trans Tech Publications, 477–480.
93. Ahmad M, Ahmad M, Ali I, et al. (2015) Temperature dependent structural and magnetic behavior of Y-type hexagonal ferrites synthesized by sol-gel autocombustion. *J Alloy Compd* 651: 749–755.
94. Farzin YA, Mirzaee O, Ghasemi A (2016) Synthesis behavior and magnetic properties of Mg–Ni co-doped Y-type hexaferrite prepared by sol-gel auto-combustion method. *Mater Chem Phys* 178: 149–159.
95. Odeh I, El Ghanem HM, Mahmood SH, et al. (2016) Dielectric and magnetic properties of Zn-substituted Co_2Y barium hexaferrite prepared by sol–gel auto combustion method. *Physica B* 494: 33–40.

96. Know HJ, Shin JY, Oh JH (1994) The microwave absorbing and resonance phenomena of Y type hexagonal ferrite microwave absorber. *J Appl Phys* 75:6109 .
97. Xu F, Bai Y, Jiang K, et al. (2012) Characterization of a Y-type hexagonal ferrite-based frequency tunable microwave absorber. *Int J Min Met Mater* 19: 453–456.
98. Xing L, Shun-kang P, Xing Z, et al. (2017) Microwave-absorbing properties of strontium ferrites prepared via sol-gel method. *Cryst Res Technol* 52: 1700057.
99. Mohsen Q (2010) Barium hexaferrite synthesis by oxalate precursor route. *J Alloy Compd* 500: 125–128.
100. Dionne GF, Oates DE, Temme DH, et al. (1996) Ferrite-superconductor devices for advanced microwave applications. *IEEE T Microw Theory* 44: 1361–1368.
101. SUZUKI T, ISSHIKI M, OGUCHI T, et al. (1991) Orientation and recording performance for Ba-ferrite tapes. *J Magn Soc Jpn* 15: S2_833–838.
102. Kong S, Zhang P, Wen X, et al. (2008) Influence of surface modification of $SrFe_{12}O_{19}$ particles with oleic acid on magnetic microsphere preparation. *Particuology* 6: 185–190.
103. Cannas C, Ardu A, Peddis D, et al. (2010) Surfactant-assisted route to fabricate $CoFe_2O_4$ individual nanoparticles and spherical assemblies. *J Colloid Interf Sci* 343: 415–422.

AIMS Press